






## Article

# Energetic [1,2,5]oxadiazolo [2,3-*a*]pyrimidin-8-ium Perchlorates: Synthesis and Characterization

Kirill V. Strizhenko <sup>1</sup>, Anastasia D. Smirnova <sup>1,2</sup>, Sergei A. Filatov <sup>2</sup>, Valery P. Sinditskii <sup>1,2</sup>, Adam I. Stash <sup>3</sup>, Kyrill Yu. Suponitsky <sup>3</sup>, Konstantin A. Monogarov <sup>4</sup>, Vitaly G. Kiselev <sup>5</sup> and Aleksei B. Sheremetev <sup>1,\*</sup>

<sup>1</sup> Zelinsky Institute of Organic Chemistry, Russian Academy of Sciences, 119991 Moscow, Russia

<sup>2</sup> Mendeleev University of Chemical Technology, 125047 Moscow, Russia

<sup>3</sup> Nesmeyanov Institute of Organoelement Compounds, Russian Academy of Sciences, 119334 Moscow, Russia

<sup>4</sup> Semenov Federal Research Center for Chemical Physics, Russian Academy of Sciences, 119991 Moscow, Russia

<sup>5</sup> Institute of Chemical Kinetics and Combustion, Russian Academy of Sciences, Siberian Branch, 630090 Novosibirsk, Russia

\* Correspondence: sab@ioc.ac.ru

**Abstract:** A convenient method to access the above perchlorates has been developed, based on the cyclocondensation of 3-aminofurazans with 1,3-diketones in the presence of HClO<sub>4</sub>. All compounds were fully characterized by multinuclear NMR spectroscopy and X-ray crystal structure determinations. Initial safety testing (impact and friction sensitivity) and thermal stability measurements (DSC/DTA) were also carried out. Energetic performance was calculated by using the PILEM code based on calculated enthalpies of formation and experimental densities at r.t. These salts exhibit excellent burn rates and combustion behavior and are promising ingredients for energetic materials.

**Keywords:** aminofurazans; fused furazans; perchlorates; energetic compound; synthesis; X-ray analysis; impact sensitivity; thermal decomposition; combustion; burning rate



**Citation:** Strizhenko, K.V.; Smirnova, A.D.; Filatov, S.A.; Sinditskii, V.P.; Stash, A.I.; Suponitsky, K.Y.; Monogarov, K.A.; Kiselev, V.G.; Sheremetev, A.B. Energetic [1,2,5]oxadiazolo [2,3-*a*]pyrimidin-8-ium Perchlorates: Synthesis and Characterization. *Molecules* **2022**, *27*, 8443. <https://doi.org/10.3390/molecules27238443>

Academic Editor: Gilbert Kirsch

Received: 7 November 2022

Accepted: 25 November 2022

Published: 2 December 2022

**Publisher's Note:** MDPI stays neutral with regard to jurisdictional claims in published maps and institutional affiliations.



**Copyright:** © 2022 by the authors. Licensee MDPI, Basel, Switzerland. This article is an open access article distributed under the terms and conditions of the Creative Commons Attribution (CC BY) license (<https://creativecommons.org/licenses/by/4.0/>).

## 1. Introduction

Most energetic materials are a mixture of substances, among which an oxidizer, fuel, binder and various corrective additives can be specified. The most widely used oxidizer is ammonium perchlorate, NH<sub>4</sub>ClO<sub>4</sub> [1–4]. In the early stages of research, compositions based on NH<sub>4</sub>ClO<sub>4</sub> included powdered metals as fuel. However, in recent years, there has been a tendency to partially or even completely replace metallic fuels in energetic materials with high-nitrogen compounds characterized by high positive enthalpies of formation.

Energetic salts with nitrogen-rich organic cations and/or anions (typically azole-based ions) are a major area for the development of high-energy materials, since salts have a high density and positive enthalpy of formation, are often thermally stable, and are not volatile [5–7]. Designing energetic salts by combining various cations and anions to achieve a specific purpose is a simple but powerful methodology. Most of these salts, however, have a strongly negative oxygen balance and, with a lack of oxidizer, form toxic or undesirable solid decomposition products [8].

When using energetic salts in combination with solid inorganic oxidizers—for example, with NH<sub>4</sub>ClO<sub>4</sub>—additional problems are observed. A metathesis reaction between NH<sub>4</sub>ClO<sub>4</sub> and energetic azole-based salts leads to the formation of new salts where the anions have been swapped. As a result, the properties of this composition could change unpredictably [9]. To overcome this disadvantage, a variety of energetic organic salts may be limited by the use of perchlorates.

The characteristics of the energetic salts are dictated by the physical and chemical features of both ions in their composition. In this light, the importance of synthesizing organic salts of perchloric acid with various cations and the study of their properties

becomes important. It is important to note that, unlike nitrates, perchlorates have a significant effect on the transformation of organic compounds [10–12], which favors the completeness of the combustion of the latter.

Due to its inherent density, positive enthalpy of formation, thermal stability, and the presence of an active oxygen atom, the 1,2,5-oxadiazole (furan) ring is an attractive building block for the development of new energetic compounds [13–17]. Significant progress has been achieved in the development of furazan-based salts, some types of which are depicted in Figure 1. Typically, the furazan moiety is located in the anionic part of the energetic salt, as in salts of nitramines **1** [18–23], perchlorylamines **2** [24], dinitromethyl **3** [25–32], tetrazolyl **4** [33–37], pyrazolo [3,4-*c*]furanates **5** [38–40], and [1,2,3]triazolo [4,5-*c*] [1,2,5]oxadiazoles **6** [41]. Cations involving the furazan ring are very rare; in the previously described salts (**7** [42] and **8** [20]), the positive charge is located in the side chain.

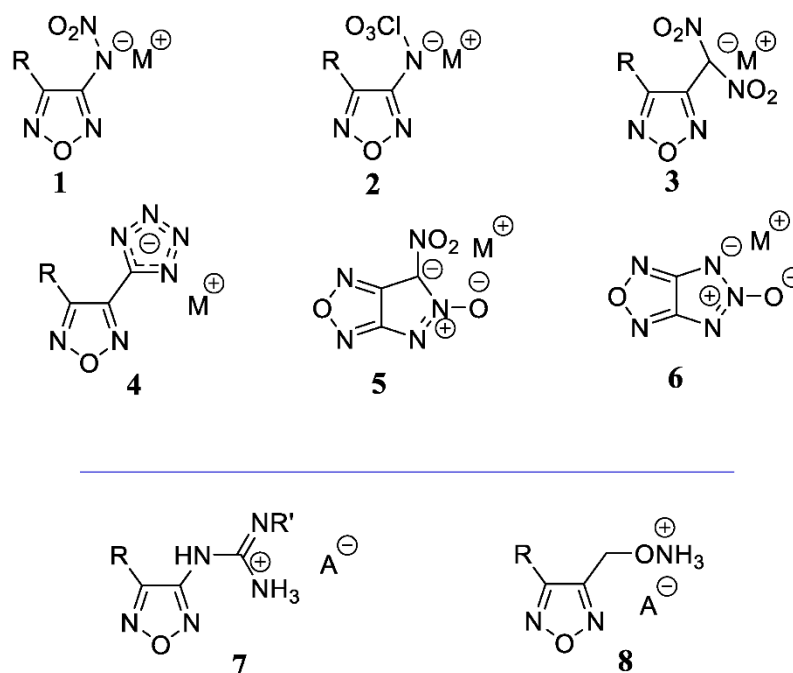


**Figure 1.** Known energetic furazan-based salts.

There is no literature precedence for energetic salts incorporating a furazan-based backbone with a positive charge on the nitrogen atom of this ring.

Although a few 2-methyl-1,2,5-oxadiazolium [43] and 1,2,5-oxadiazolo [2,3-*a*]-pyrimidinium perchlorates [44,45] were synthesized, only partial physical and spectral properties were available, but the sensitivity, thermal stability, combustion features, and explosive performance were not reported. However, these early studies have demonstrated that monocyclic salts are less accessible and more reactive.

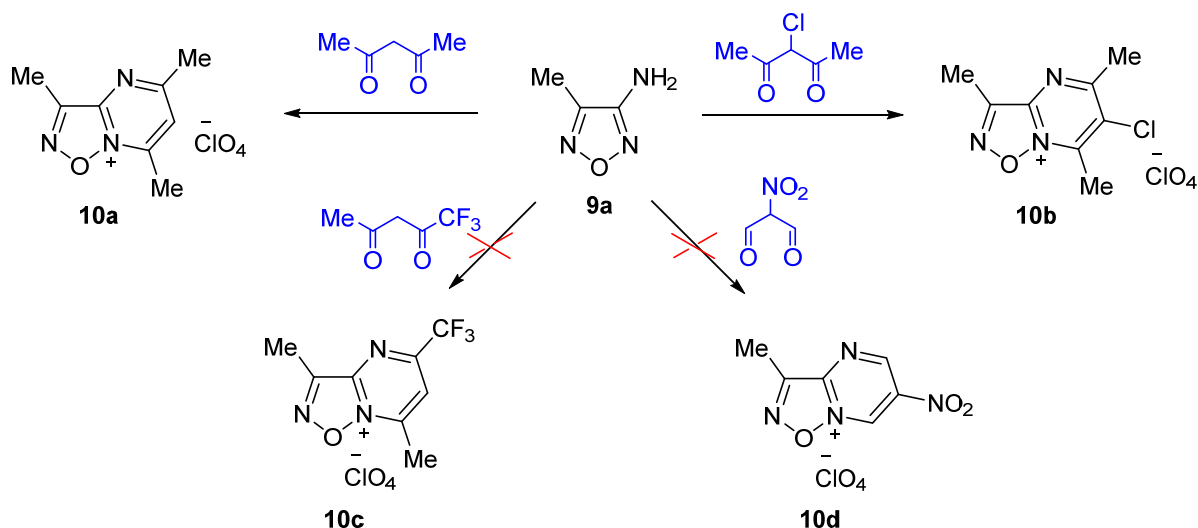
In light of the above, we report here a new, straightforward method for the synthesis of energetic 1,2,5-oxadiazolo [2,3-*a*]-pyrimidinium perchlorates, and their full characterization, including energetic properties. The only known pathway for the synthesis of 1,2,5-oxadiazolo [2,3-*a*]-pyrimidinium perchlorates is based on the reaction of 3-amino-4-*R*-furanans **9** with 1,3-dicarbonyl compounds [44]. However, an investigation of the scope and limitations of functionalized reactants has not been previously reported. Although a range of alkyl and aryl-substituted oxadiazolo [2,3-*a*]-pyrimidinium perchlorates have been prepared by this approach, there have been no examples bearing explosophoric groups [46] so far.

## 2. Results

### 2.1. Synthesis

Readily available 3-amino-4-methylfuran (9a) [47] became our model precursor of choice. There is a literature report [44] on the synthesis of 1,2,5-oxadiazolo [2,3-*a*]-pyrimidinium perchlorate 10a from compound 9a and pentane-2,4-dione in a mixture of AcOH and HClO<sub>4</sub>, but no synthetic details are given. In our hands, such a procedure turned out to be somewhat unpredictable; the yield of the final 1,2,5-oxadiazolo [2,3-*a*]-pyrimidinium perchlorate 10a was relatively low (only 23% vs. 73% reported earlier).

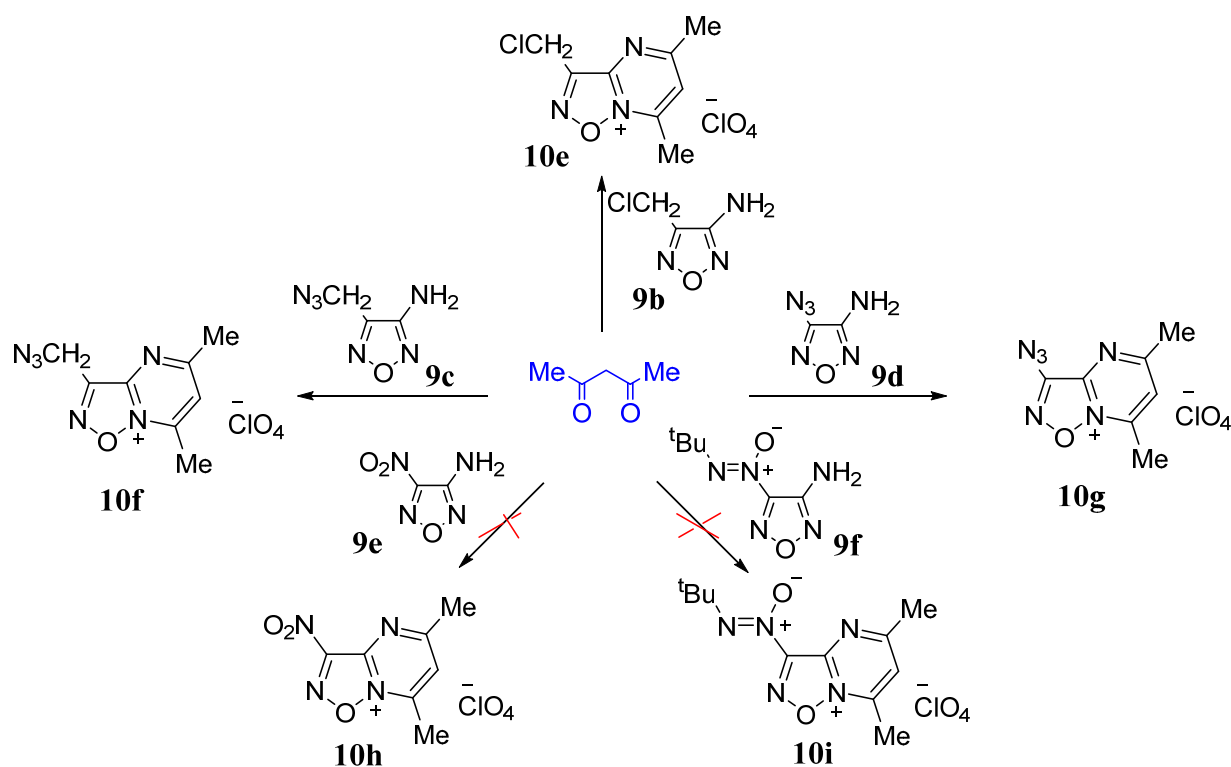
After several experiments, we found that replacing AcOH in the reaction mixture with Ac<sub>2</sub>O improved the conversion significantly and gave a 44% yield of the product 10a (Scheme 1). A change in dehydrating agent from Ac<sub>2</sub>O to (CF<sub>3</sub>CO)<sub>2</sub>O allowed us to increase the yield up to 87%. It has been suggested that the solubility of the product 10 in the reaction mixture is the most important in this process. (CF<sub>3</sub>CO)<sub>2</sub>O is completely unnecessary as a reagent, and the much cheaper and easier-to-handle trifluoroacetic acid was employed instead. Gratifyingly, treatment of amine 9a with pentane-2,4-dione in a mixture of 58% HClO<sub>4</sub> and CF<sub>3</sub>CO<sub>2</sub>H at room temperature gave the cyclocondensation product 10a in 3 h. Thus, without any complicated workup, the desired product was isolated in 71% yield and >99% purity through simple filtration and washing.



**Scheme 1.** Reaction of 3-amino-4-methylfuran (9a) with 1,3-dicarbonyl compounds.

With the optimized conditions developed, we explored the scope of the method with a variety of 1,3-dicarbonyl compounds and aminofurazans bearing explosophoric groups. A 1,3-dicarbonyl compound with one halogen, namely 3-chloropentane-2,4-dione, furnished the desired product 10b in a good yield (85%). The use of 1,3-dicarbonyl compounds possessing strongly electron-withdrawing substituents, e.g., trifluoromethyl or nitro groups (Scheme 1), failed to give the corresponding bicycles 10c and 10d.

Scheme 2 shows the results of applying our optimized cyclocondensation conditions to a range of aminofurazans. Aminofurazans bearing a functionalized methyl group, 3-amino-4-chloromethylfuran (9b) [48] and 3-amino-4-azidomethylfuran (9c) [48], were equally effective as the model compound 9a, with excellent yields (ca. 95%) being obtained for pentane-2,4-dione in the HClO<sub>4</sub>/CF<sub>3</sub>CO<sub>2</sub>H system. Moreover, 3-amino-4-azidofuran (9d) [49,50] was a good substrate for the reaction and gave the target product 9e in 71% yield. Synthesis of 1,2,5-oxadiazolo [2,3-*a*]-pyrimidinium perchlorate failed in cases where the starting furazan had a very strong electron-withdrawing substituent: reactions with 3-amino-4-nitrofuran 9e [51] or with 3-amino-4-*tert*butylazoxyfuran 9f [52] did not give the desired salts 10h and 10i. Only recovery of the starting materials from the reaction mixture was achieved.



**Scheme 2.** Reaction of pentane-2,4-dione with aminofurazans.

With the exception of compound **10a**, all perchlorates prepared in this way are new, and the structures of the products have been confirmed by elemental analyses, IR, and  $^1\text{H}$ ,  $^{13}\text{C}$ ,  $^{15}\text{N}$ , and  $^{35}\text{Cl}$  NMR spectroscopy. The  $^1\text{H}$ ,  $^{13}\text{C}$  and  $^{15}\text{N}$  chemical shift assignments were determined by using  $^1\text{H}$  selective NOE,  $^1\text{H}$ - $^{13}\text{C}$  HSQC,  $^1\text{H}$ - $^{13}\text{C}$  HMBC, and  $^1\text{H}$ - $^{15}\text{N}$  HMBC experiments. In the  $^{35}\text{Cl}$  NMR spectrum, the characteristic chlorine signal of the perchlorate anion appeared at 1012 ppm, which is close to the reported values of similar compounds [53]. For clarity, the compound of this study, together with relevant NMR parameters, is depicted in Figure 2.

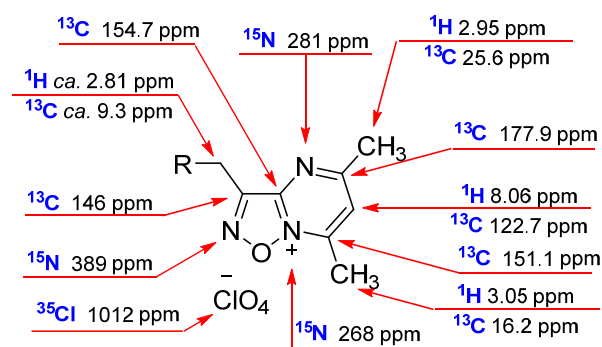


**Figure 2.** Typical  $^1\text{H}$ ,  $^{13}\text{C}$ ,  $^{15}\text{N}$ , and  $^{35}\text{Cl}$  NMR shifts of 1,2,5-oxadiazolo [2,3-*a*]-pyrimidin-1-ium perchlorates.

## 2.2. X-ray Analysis

The X-ray crystal structures of perchlorates **10a**, **10f**, and **10g**, differing only by the substituent at the 1,2,5-oxadiazole ring, are shown in Figures 3 and 4. Both symmetrically independent molecules of methyl compound **10a** adopt a planar structure. Azido groups in three symmetrically independent molecules of **10g** are rotated ca.  $17.6^\circ$ – $26.7^\circ$  out of the plane of the bicyclic backbone. For compound **10f**, the  $\text{CH}_2\text{N}_3$  substituent deviates even more significantly from the plane of the heterocycle (the C2–C1–C8–N4 torsion angle is equal to  $59.7(2)^\circ$ ).

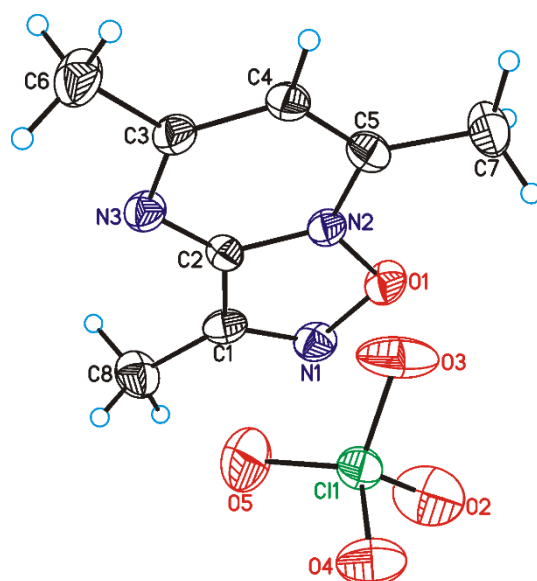


**Figure 3.** General view of Me compounds **10a** showing atomic numbering. Thermal ellipsoids are given at 50% probability level. The first symmetrically independent molecule is shown.

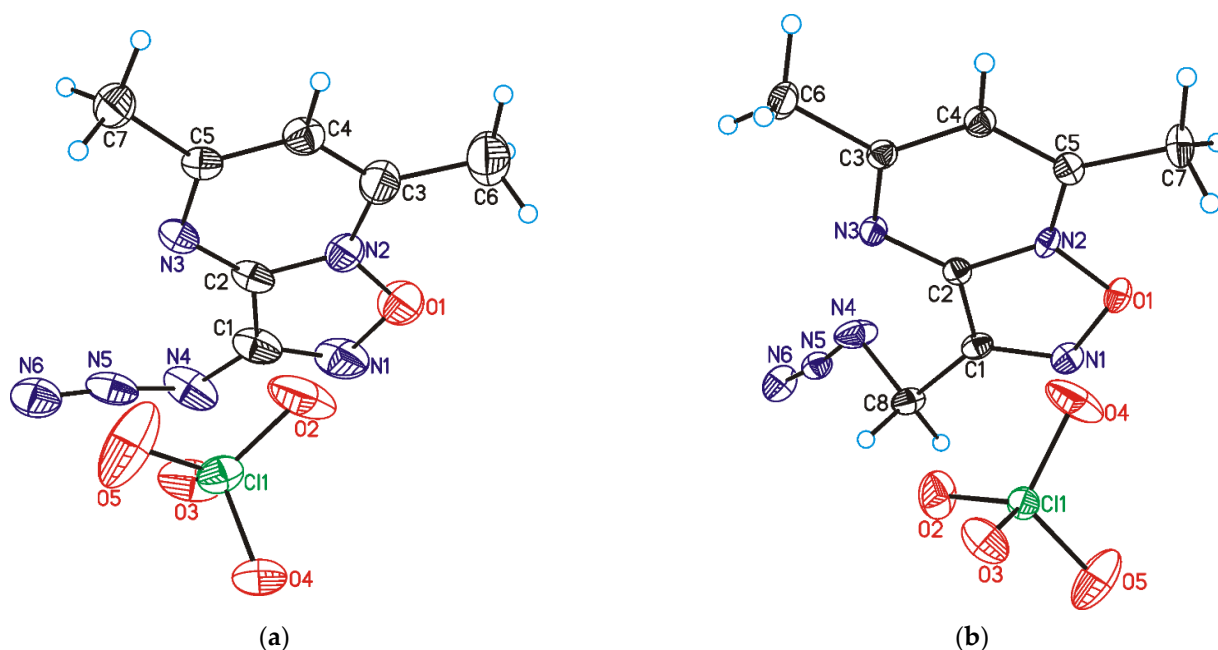


**Figure 4.** General view of azido compounds **10g** (a) and **10f** (b) showing atomic numbering. Thermal ellipsoids are given at 50% probability level. For **10g**, the first symmetrically independent molecule is shown.

The N–O bond lengths in the 1,2,5-oxadiazole ring, which are usually the most sensitive to the influence of substituents [54–56], are distributed so that the O1–N2 bond is significantly shorter than the other one in all three compounds. The difference in these bonds  $\Delta(\text{NO})$  (for **10a** and **10g**, the average value over symmetrically independent molecules is used) increases in the order of the decreasing electron-withdrawing effect of the substituent at the C1 atom (the  $\Delta(\text{NO})$  is 0.022, 0.026, 0.035 Å for compounds **10g**, **10f**, and **10a**, respectively).

For all three compounds, the molecules in the crystal are linked together by O... $\pi$ , C–H...O(N), and van-der-Waals interactions. As expected, most of them are observed between anions and cations, as depicted in Figures 5–7. In the cases of azido compounds

(Figures 6 and 7), each anion (except for one in **10g**, Figure 6) is linked to four cations by means of  $O \cdots \pi$  and  $C-H \cdots O$  interactions, and the interaction patterns are quite similar for both compounds. In the case of Me derivatives (Figure 5), each anion is surrounded by three counterions. In all three structures, the cation  $\cdots$  cation interactions are caused by van-der-Waals forces and weak  $C-H \cdots N$  hydrogen bonds, while no anion  $\cdots$  anion contacts are observed.

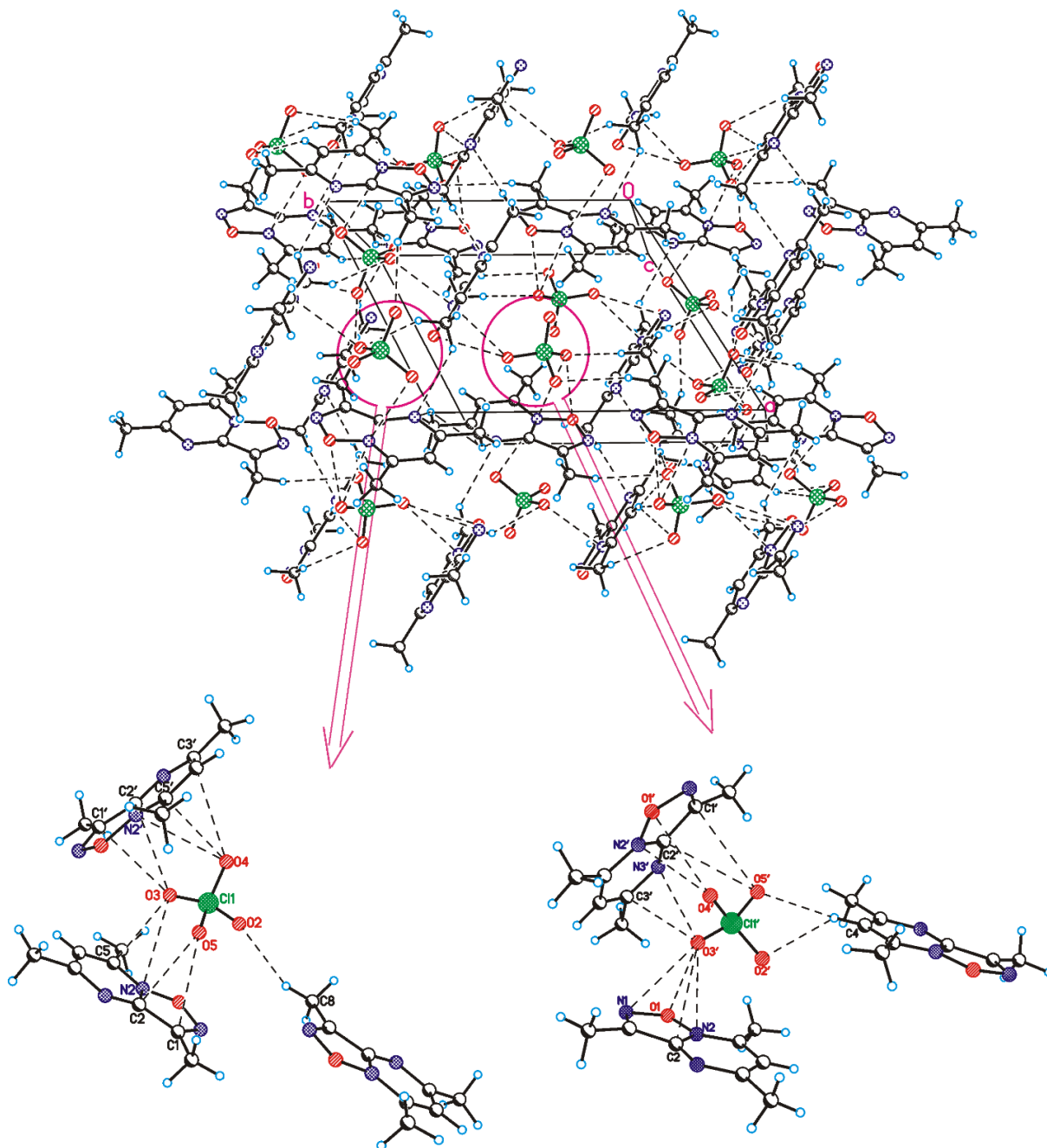


**Figure 5.** Crystal packing fragment of compound **10a**.  $C-H \cdots N$  cation  $\cdots$  cation and  $C-H \cdots O$  and  $O \cdots \pi$  anion  $\cdots$  cation interactions are shown by dashed lines. Detailed view of anion  $\cdots$  cation interactions is provided at the bottom. Minor part of the disorder is omitted for clarity.



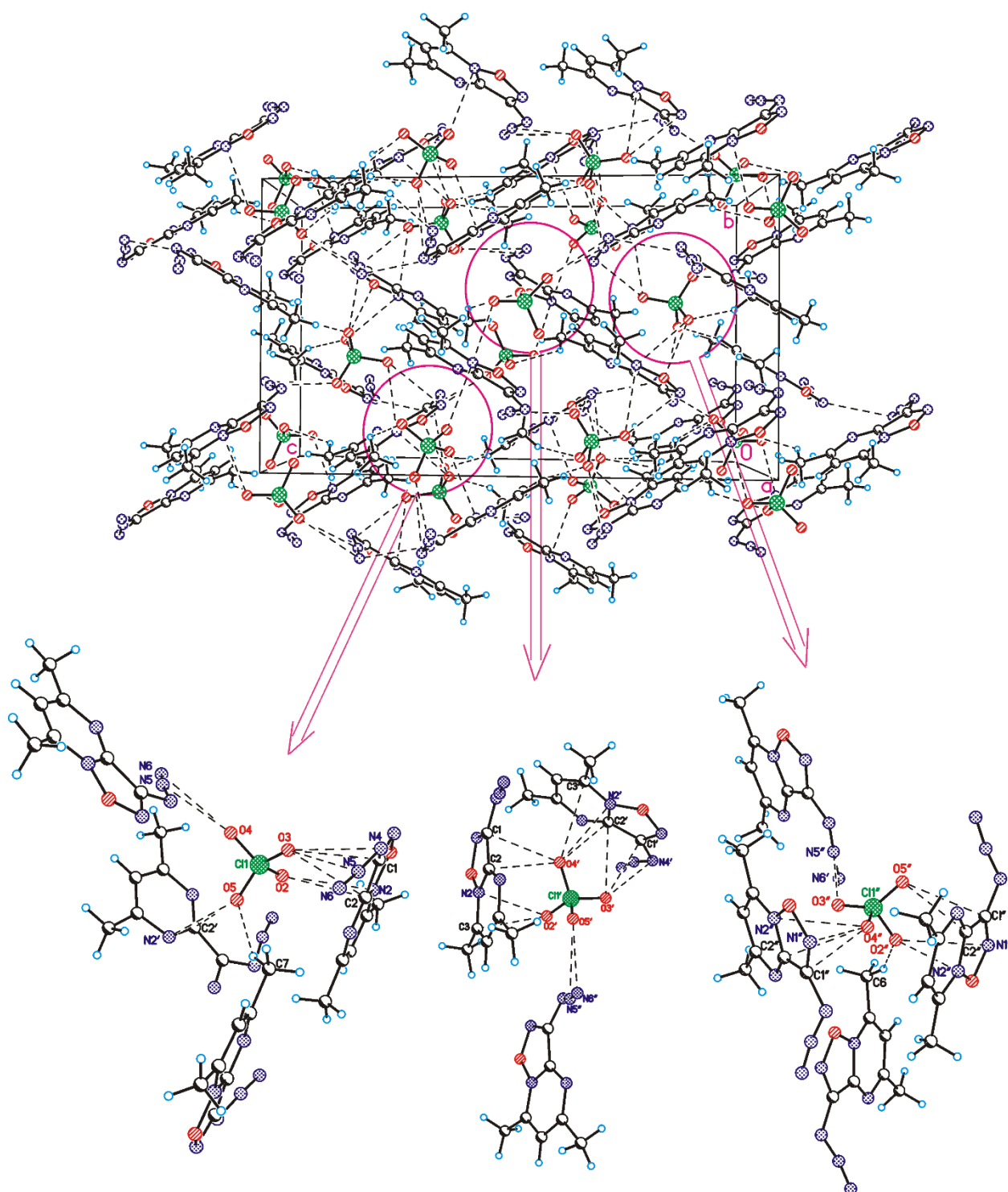


**Figure 6.** Crystal packing fragment of compound **10g**. C–H ... N cation–cation and C–H ... O and O ...  $\pi$  anion ... cation interactions are shown by dashed lines. Detailed view of anion ... cation interactions is provided at the bottom. Minor part of the disorder is omitted for clarity.

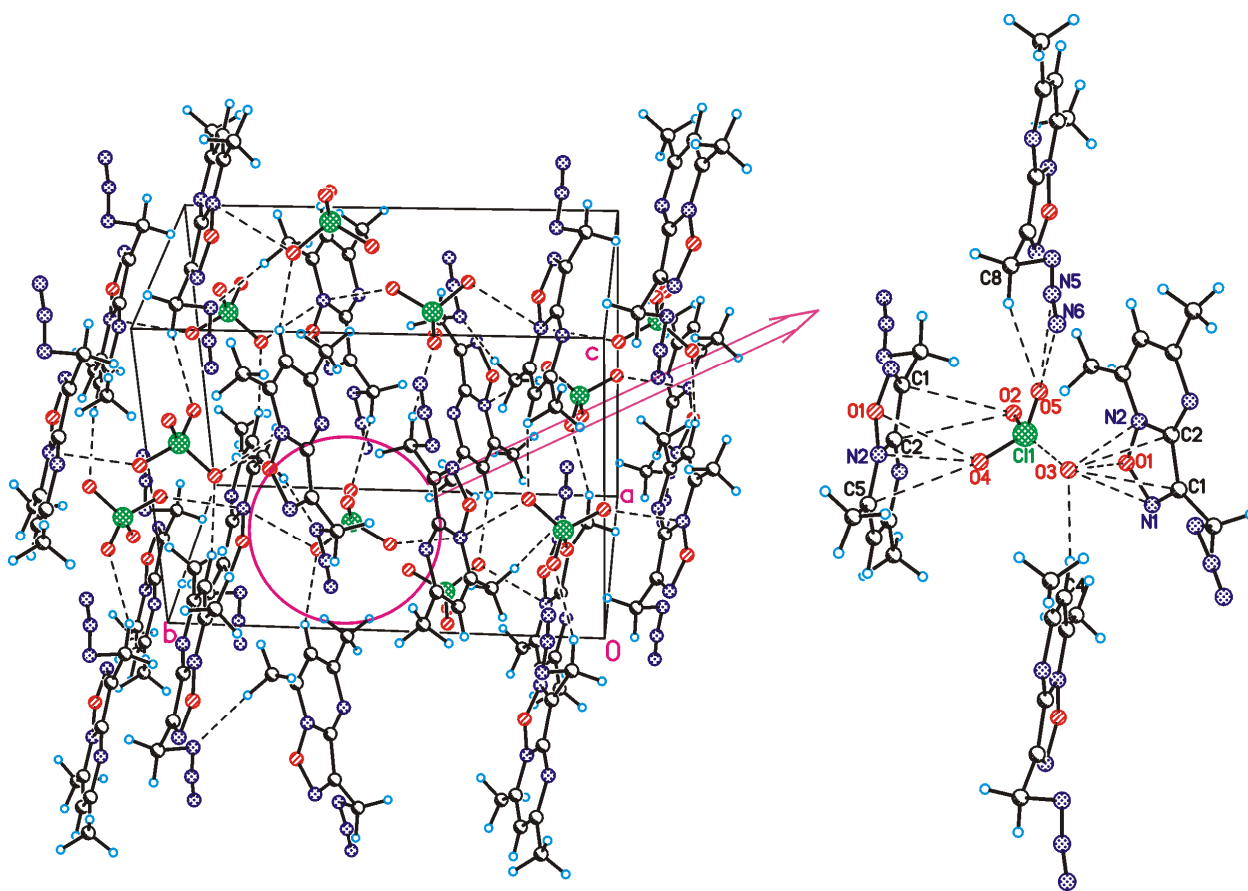


**Figure 7.** Crystal packing fragment of compound **10f**. C–H ... N cation ... cation and C–H ... O and O ...  $\pi$  anion ... cation interactions are shown by dashed lines. Detailed view of anion–cation interactions is provided on the right side.

As expected, the density of Me compound **10a** ( $1.549 \text{ g cm}^{-3}$  at 100 K) is lower than that of its azido analogues. However, unexpectedly, the density of the azido derivative **10g** turned out to be lower than that of the azidomethyl compound **10f** ( $1.611$  vs.  $1.649 \text{ g cm}^{-3}$  at 100 K). Probably due to the significant disorder in the structure **10f**, disordered fragments occupy a larger volume, which leads to a decrease in density.

### 2.3. Initial Safety Testing

For initial safety testing, the impact (IS) and friction (FS) sensitivities of perchlorates **10a**, **10e–10g** were measured. The sensitivity measurements were carried out using common BAM techniques and compared to tetrazene, which is considered as the benchmark primary metal-free explosive (Table 1). Compound **10a** bearing the methyl group at 1,2,5-oxadiazole ring and compound **10e** with the chloromethyl group showed similar impact and friction sensitivities. A change in the position of the chlorine atom—namely, its transfer from the methyl group to the pyrimidine ring, as in compound **10c**—slightly reduces the sensitivity to friction and increases the thermal stability. Unexpectedly, when the chloromethyl group was replaced with an azidomethyl group, as in compound **10f**, the sensitivity decreased to 2.6 J. The friction sensitivity of compound **10a** is two times lower than that of the chlorine derivative **10e**, and two times higher than that of azidomethyl compound **10f**. The primary differential scanning calorimetric (DSC,  $5 \text{ }^{\circ}\text{C min}^{-1}$ ) tests are also presented in Table 1.



**Table 1.** Explosive sensitivity for compounds of this study in comparison with tetrazene.

Compound	Formula	IS, <sup>a</sup> J	FS, <sup>b</sup> N	DSC, <sup>c</sup> °C
<b>10a</b>	C <sub>8</sub> H <sub>10</sub> Cl <sub>1</sub> N <sub>3</sub> O <sub>5</sub> (263.63)	2.0 ± 0.4	32 ± 6	212
<b>10b</b>	C <sub>8</sub> H <sub>9</sub> Cl <sub>2</sub> N <sub>3</sub> O <sub>5</sub> (298.08)	2.1 ± 0.8	36 ± 8	177
<b>10e</b>	C <sub>8</sub> H <sub>9</sub> Cl <sub>2</sub> N <sub>3</sub> O <sub>5</sub> (298.08)	2 ± 1	60 ± 30	207
<b>10f</b>	C <sub>8</sub> H <sub>9</sub> Cl <sub>1</sub> N <sub>6</sub> O <sub>5</sub> (304.65)	2.6 ± 1.1	16 ± 8	142
<b>10g</b>	C <sub>7</sub> H <sub>7</sub> Cl <sub>1</sub> N <sub>6</sub> O <sub>5</sub> (290.62)	1.0 ± 0.3	5.9 ± 0.8	136
<b>tetrazene</b>	C <sub>2</sub> H <sub>8</sub> N <sub>10</sub> O <sub>1</sub> (188.15)	3 ± 2	<5	127

<sup>a</sup> Impact sensitivity (STANAG 4489). <sup>b</sup> Friction sensitivity (STANAG 4487). <sup>c</sup> Onset decomposition temperature (DSC, 5 °C min<sup>−1</sup>).

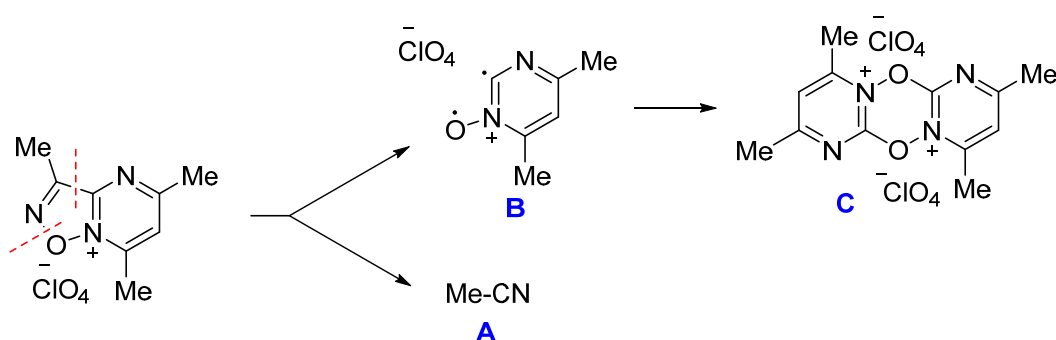
All perchlorates in this study are more thermally stable than tetrazene, slightly exceeding it in impact sensitivity, but less sensitive to friction. Compound **10g** with the azido group at the 1,2,5-oxadiazole ring is the most impact- and friction-sensitive in this series of salts.

#### 2.4. Thermal Analysis

Since the azide compounds **10f** and **10g** are the most energetic, we continued to characterize them and the model compound **10a** from the point of view of their decomposition under heating. The thermal stabilities of the compounds were determined by DSC and thermogravimetric analysis (TGA) measurements scanning at 10 °C min<sup>−1</sup>. The model compound **10a** decomposes without melting, and the maximum heat release was observed at 218–219 °C, which is comparable to that of common RDX. However, decomposition proceeds very intensively; an acceptable DSC curve can only be obtained on a sample less than 0.2 mg. In TGA measurements, the weight loss occurring at this temperature is approximately 19%, which is close to MeCN release (15.6%), as previously observed for 1,2,5-oxadiazoles [48,57–62]. Further weight loss is observed after 280 °C, which characterizes the second stage of decomposition (see Supplementary Materials, Figure S1).

Decomposition of the model compound **10a** under isothermal conditions was performed using a Bourdon glass compensation pressure gauge [63] in the temperature range of 160–180 °C. The ratio of the weight of the sample to the volume of the reaction vessel (m/V) was  $\sim 1 \times 10^{-3}$  g cm<sup>3</sup>. The destruction of **10a** under this condition proceeds with an acceleration in time, which, at temperatures above 160 °C, turns into a degenerate thermal explosion (Supplementary Materials, Figure S4). During decomposition, only 60–95 cm<sup>3</sup> g or 0.7–1.11 moles of colorless gaseous products were released from a mole of the initial **10a**, most of which condenses during cooling. After stopping the process, a dark brown powder remains at the bottom of the vessel. An absorption band of the ClO<sub>4</sub><sup>−</sup> (1100 cm<sup>−1</sup>) anion was observed in the IR spectrum of the residue.

A probable mechanism of the initial destruction stage of salt **10a** is proposed in Scheme 3. This is consistent with the typical decomposition mechanism of 1,2,5-oxadiazoles previously observed for various compounds of this heterocycle [57,58,60,62]. The breaking of the two bonds of the 1,2,5-oxadiazole ring (indicated in the Scheme 3) gives the nitrile product **A** as a result of the typical ring disintegration process. Rapid intermolecular cyclization of the resulting reactive monocyclic intermediate **B** leads to a tricyclic intermediate **C**, capable of further transformations.



**Scheme 3.** The proposed first stage of decomposition of salt **10a**.

X-ray diffraction analysis of **10a** shows that the O1–N2 bond is significantly shorter than the other O1–N1 bond of the 1,2,5-oxadiazole ring, which explains the breaking of the latter. The IR spectrum of the final residue includes bands corresponding to C=N bonds ( $1640$ ,  $1590$ ,  $1430\text{ cm}^{-1}$ ), as well as a strong absorption band of the  $\text{ClO}_4^-$  anion ( $1100\text{ cm}^{-1}$ ).

The main heat effect is achieved due to the formation of C–O bonds during the formation of tricyclic compound **C**. The formation of two new C–O bonds, even without taking into account the change in the enthalpy part, makes it possible to estimate the heat effect at  $746\text{ J g}^{-1}$ , which is in good agreement with the DSC data ( $1164\text{ J g}^{-1}$ ).

Compound **10f** bearing the  $\text{CH}_2\text{N}_3$  group at the 1,2,5-oxadiazole ring melts at  $142\text{ }^\circ\text{C}$  (enthalpy of melting  $L_m > 23\text{ J g}^{-1}$ ), and, immediately after this, the exothermic stage of decomposition begins (Supplementary Materials, Figure S3). Decomposition of **10f** proceeds in two stages. At the first, occurring at  $143\text{--}180\text{ }^\circ\text{C}$  with a maximum at  $159\text{ }^\circ\text{C}$  ( $1438\text{ J g}^{-1}$ ), the weight reduction was 27.6%, which corresponds to a loss of  $\text{N}_3\text{CH}_2\text{CN}$  (26.9%), as a result of the breaking of two bonds in the 1,2,5-oxadiazole ring, similar to what was observed for **10a** (Scheme 3). With such isothermal decomposition of **10f**, the gas release is  $120\text{ cm}^3\text{ g}^{-1}$  or  $1.66\text{ mol}$  per mol of the compound (see Supplementary Materials, Figure S6). It is obvious that, in this case, there is also a decomposition of the azide group.

Compound **10g** bearing an electron-withdrawing azide group at the 1,2,5-oxadiazole ring is slightly less thermally stable. When heated using a  $10\text{ }^\circ\text{C min}^{-1}$  ramp rate, it decomposes in the range of  $140\text{--}164\text{ }^\circ\text{C}$  (maximum heat release of  $150\text{ }^\circ\text{C}$ ). Total energy of the decomposition was  $2061\text{ J g}^{-1}$ . Weight loss at this stage reaches 54%, which indicates a deeper decomposition process than is shown in Scheme 3. On the DSC curve, there is another area with weaker heat release at  $325\text{ }^\circ\text{C}$ , where the weight loss is 21% (see SI, Figure S2).

The decomposition of all compounds of this study under isothermal conditions proceeds with an acceleration in time, and, after completion, a dark brown powder remains at the bottom of the vessel. Here, decomposition was carried out at temperatures below the onset decomposition temperature registered in the DSC. The observed acceleration is associated with the submelting of samples. The analysis of such gas release curves makes it possible to simultaneously determine two decomposition constants, (i) in the solid phase ( $k_s$ ) and (ii) in the liquid phase ( $k_{\text{liq}}$ ). The obtained data are summarized in Table 2 and Figure S7 (see Supplementary Materials). The activation energies of decomposition in the solid phase are relatively low ( $145\text{--}164\text{ kJ mol}^{-1}$ ) and, within the measurement error ( $\pm 10\text{ kJ mol}^{-1}$ ), practically do not change during the transition to the liquid phase ( $152\text{--}157\text{ kJ mol}^{-1}$ ). In general, there are two trends in the data in Table 2. The first is that the decomposition in the liquid phase is much faster than in the solid phase. The second trend is that the rate decomposition constants of the perchlorates of this study, both in the solid phase and in the melt phase, and the Hammett constants of the substituent at the 1,2,5-oxadiazole ring, increase synchronously. A good correlation between the rate of thermal decomposition and the Hammett constant indicates a unified mechanism of the initial stage of destruction of these compounds.

**Table 2.** Parameters of the Arrhenius equation for perchlorates and benchmark tetrazene.

Sampl	Substituent	$\sigma_I^a$	State	T, °C	logA <sup>b</sup>	$E_a^c$ , kJ mol <sup>−1</sup>	$k_{150C}^d$ , s <sup>−1</sup> × 10 <sup>4</sup>
10a	CH <sub>3</sub>	−0.07	Solid	160–180	14.5	164	0.015
10f	N <sub>3</sub> CH <sub>2</sub>	0.11	Solid	110–120	14.3	157	0.084
10g	N <sub>3</sub>	0.33	Solid	80–105	15.0	145	12
Tetrazene <sup>e</sup>			Solid	115–125	18.7	163	372
	CH <sub>3</sub>	−0.07	Liquid	170–180	18.7 <sup>f</sup>	183 <sup>f</sup>	1.1
	N <sub>3</sub> CH <sub>2</sub>	0.11	Liquid	110–130	17.6	157	163
	N <sub>3</sub>	0.33	Liquid	90–110	18.8	152	530

<sup>a</sup> Hammett constant [64]. <sup>b</sup> The Arrhenius preexponential factor. <sup>c</sup> Activation energy. <sup>d</sup> Rate constant at 150 °C. <sup>e</sup> Data from non-isothermal conditions [65]. <sup>f</sup> Estimated values for two points.

Since the decomposition of compounds proceeds with acceleration, the data obtained under non-isothermal conditions (see Supplementary Materials, Table S1) give the formal kinetics of the total process. Previously, the decomposition of tetrazene was described only under non-isothermal conditions [65]. Comparison of the decomposition kinetics under the same conditions (see Supplementary Materials, Figure S7) reveals that the perchlorates of this study are superior to tetrazene in thermal stability. The decomposition rate constant of tetrazene at 150 °C is several orders of magnitude higher than that of the studied perchlorates (Table 2).

### 2.5. Combustion

The combustion behaviors of the perchlorates were studied on pressed charges in polyurethane tubes (4 mm inner diameter and ca. 8 mm length). However, at elevated pressures, combustion in the tubes turns into an explosion. For example, the compound **10g** could be burned only at a pressure below 3 MPa. For compound **10f**, a clear result was obtained only when using charges in the form of thin (~1 mm) plates pressed to a high density. The use of such charges avoids the penetration of hot gases into the pores and prevents the transition of layer-by-layer combustion in convective ones. As a result, compound **10f** was able to burn even at high pressures (Figure 8 and Table 3).

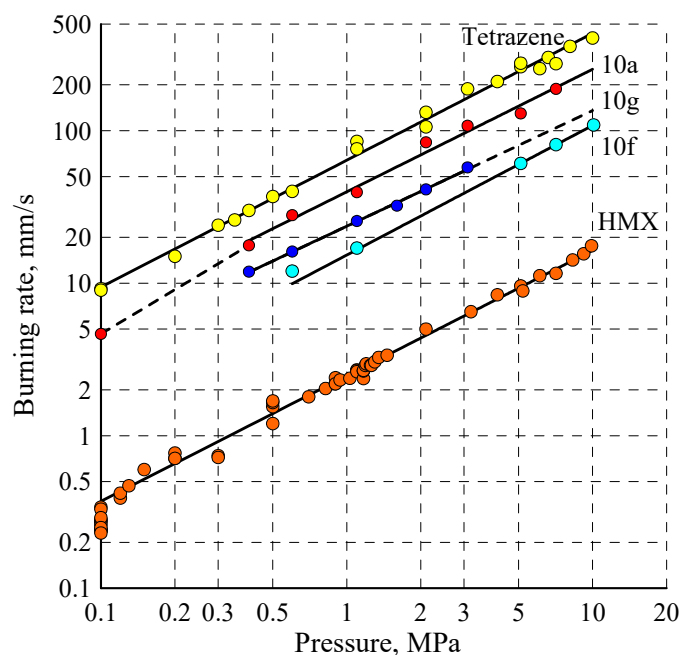


**Figure 8.** Comparison of burning rates at different pressures for **10a**, **10f**, and **10g** with tetrazene and HMX. Dotted line is extrapolation.

**Table 3.** The combustion parameters of perchlorates and benchmark compounds.

Compound	$\Delta p$ , <sup>a</sup> MPa	Burning Rate $r_b = Ap^n$		$r_{b10}$ , <sup>d</sup> mm s <sup>−1</sup>
		A <sup>b</sup>	n <sup>c</sup>	
<b>10a</b>	0.1–0.4	42.7	0.96	250
	0.4–10.0	39.7	0.80	
<b>10g</b>	0.1–0.4	14.4	0.21	139
	0.4–10.0	23.6	0.76	
<b>10f</b>	5.1–10.0	15.3	0.85	109
<b>Tetrazene</b>	0.1–10.0	64.0	0.83	435
<b>HMX</b>	0.1–10.0	2.47	0.82	16

<sup>a</sup> Pressure range. <sup>b</sup> Empirical coefficient. <sup>c</sup> Pressure exponent in the burning rate law. <sup>d</sup> Calculated burning rate at 10 MPa.

As can be seen from Figure 8, the burning rates of compounds **10** are significantly higher than HMX (1,3,5,7-tetranitro-1,3,5,7-tetraazacyclooctane) [66] and comparable to the burning rates of tetrazene [67].

Remarkably, the burning rates of the perchlorates of this study increase in the following order: **10f** < **10g** < **10a**. However, a similar trend is observed in terms of increasing stability; that is, the decomposition rate of these perchlorates decreases. This result demonstrates a drastic difference from the usual correlations, when an increase in thermal stability leads to a decrease in the burning rate. It can be assumed that the thermolysis of perchlorates, which proceeds with the formation of gaseous products, is a process that determines the temperature of their surfaces during combustion. In this case, the more stable the perchlorate, the higher the temperature of its surface during combustion. If the burning rate is determined by reactions in the condensed phase, which is typical for compounds with low thermal stability [68], the surface temperature at which the leading combustion reaction takes place will be a more significant factor than the decomposition rate.

## 2.6. Explosive Performance

To evaluate the performance of these newly synthesized compounds, the enthalpies of formation were calculated (see Supplementary Materials) and are summarized in Table 4. Even for the model compound **10a** bearing three ballast methyl groups, the enthalpy of formation is positive and there is +0.56 kJ g<sup>−1</sup>, which is twice as high as that of benchmark 1,3,5-trinitro-1,3,5-triazinane (RDX; +0.32 kJ g<sup>−1</sup>). As expected, the introduction of an azide group into one methyl group, and, moreover, the replacement of the methyl group with an azide group, significantly increases the enthalpy of formation, which exceeds the value for tetrazene [69]. This is clearly seen in Table 4. It is obvious that the further replacement of the remaining methyl groups with explosophoric substituents will make it possible to design more effective target products.

**Table 4.** Explosive performance for compounds of this study in comparison with tetrazene.

Compound	Formula Mw	$d^{20}$ , <sup>a</sup> g cm <sup>−3</sup>	$\alpha$ <sup>b</sup>	$\Delta_f H^0$ , <sup>c</sup> kJ mol <sup>−1</sup> (kJ g <sup>−1</sup> )	$D$ , <sup>d</sup> m s <sup>−1</sup>	$P_{C-J}$ , <sup>e</sup> GPa
<b>10a</b>	C <sub>8</sub> H <sub>10</sub> Cl <sub>1</sub> N <sub>3</sub> O <sub>5</sub> (263.63)	1.502	0.262	+147.1 (+0.56)	6400	19
<b>10f</b>	C <sub>8</sub> H <sub>9</sub> Cl <sub>1</sub> N <sub>6</sub> O <sub>5</sub> (304.65)	1.599	0.268	+552.8 (+1.81)	7000	25
<b>10g</b>	C <sub>7</sub> H <sub>7</sub> Cl <sub>1</sub> N <sub>6</sub> O <sub>5</sub> (290.62)	1.562	0.314	+557.2 (+1.92)	7000	24
<b>Tetrazene</b>	C <sub>2</sub> H <sub>8</sub> N <sub>10</sub> O <sub>1</sub> (188.15)	1.635	0.125	+156 [69] (+0.83)	7600	20

<sup>a</sup> Density at room temperature. <sup>b</sup> Oxygen coefficient. For a compound with the molecular formula of C<sub>x</sub>H<sub>y</sub>Hal<sub>v</sub>N<sub>w</sub>O<sub>z</sub>,  $\alpha = (z + v/2)/(2x + y/2)$ . A compound with a > 1 is an oxidizer. <sup>c</sup> Calculated enthalpy of the formation for solid state. <sup>d</sup> Detonation velocity at maximal density. <sup>e</sup> Detonation pressure.

With the crystal density and enthalpy of formation data in hand, the explosive performance of perchlorates was demonstrated with the refined empirical methods implemented in the PILEM code [70]. Since the salts in Table 4 are more than two times poorer in oxygen than RDX ( $\alpha = 0.667$ ), their detonation velocities are lower than those of RDX ( $D = 8850 \text{ m s}^{-1}$ ), close to that of trinitrotoluene (TNT,  $D = 6663 \text{ m s}^{-1}$ ), and slightly lower than that of tetrazene.

The results presented in Tables 2 and 4 show that compounds **10f** and **10g** bearing  $\text{CH}_2\text{N}_3$  and  $\text{N}_3$  groups, respectively, have similar performance with respect to detonation velocity and detonation pressure, whereas **10f** is less sensitive to impact and friction. This feature can be used for the further tuning of the [1,2,5]oxadiazolo [2,3-*a*]pyrimidin-8-ium backbone.

### 3. Materials and Methods

**Caution:** Although we have encountered no difficulties during preparation and handling of these products, they are potentially explosive energetic materials. Manipulations must be carried out by using appropriate standard safety precautions.

Most of the reagents and starting materials were purchased from commercial sources and used without additional purification. The starting 3-amino-4-methylfurazan (**9a**) [47], 3-amino-4-chloromethylfurazan (**9b**) [48], 3-amino-4-azidomethylfurazan (**9c**) [48], 3-amino-4-azidofurazan (**9d**) [49,50], 3-amino-4-nitrofurazan **9e** [51], and 3-amino-4-*tert*-butylazoxyfurazan **9f** [52] were synthesized by using previously reported procedures.

IR spectra were recorded on a BrukerALPHA instrument in KBr pellets. The  $^1\text{H}$  and  $^{13}\text{C}$ ,  $^{14}\text{N}$  spectra were recorded on a Bruker AM-300 instrument (300.13, 75.47, and 21.69 MHz, respectively) at 299 K. The chemical shifts of  $^1\text{H}$  and  $^{13}\text{C}$  nuclei were reported relative to TMS ( $^1\text{H}$  and  $^{13}\text{C}$ , 0.00 ppm).  $^1\text{H}$ - $^{15}\text{N}$  HMBC experiments were run to measure the  $^{15}\text{N}$  chemical shifts ( $^{15}\text{N}$ , relative to liquid  $\text{NH}_3$ , 0.00 ppm). Elemental analysis was performed on a PerkinElmer 2400 Series II instrument. Analytical TLC was performed using commercially pre-coated silica gel plates (Kieselgel 60 F<sub>254</sub>), and visualization was effected with short-wavelength UV light.

Thermal stability was studied by differential scanning calorimetry (DSC) using a Mettler Toledo DSC 822e module. The sample (1–2 mg) was weighed in an aluminum crucible (40  $\mu\text{L}$ ), sealed under air with a press, and then pierced with a needle to leave two holes with a diameter of ca. 1 mm. The decomposition of a sample was carried out in a nitrogen atmosphere at a purge rate of 50  $\mu\text{L min}^{-1}$ . The temperature of the onset of intense decomposition ( $T_{\text{onset}}$ ) was taken as the temperature determining thermal stability. The samples were subjected to thermostating in the measuring cell at a temperature of 25 °C for 30 min before the start of measurements.

Impact and friction sensitivities were measured with a BAM-type apparatus in a series of experiments according to STANAG procedures [71,72].

The burning rate was determined in a constant-pressure device (Crawford bomb) with a volume of 2 L in a nitrogen atmosphere. The combustion process of the sample was recorded using a pressure strain gauge, which transmitted the signal to a digital oscilloscope. The start and end times of combustion were determined from oscillograms. The burning rate was calculated by dividing the sample height by the burning time and was related to the mean integral pressure during the experiment. The error in determining the burning rate did not exceed 3%.

**Single-Crystal X-ray Diffraction Study.** The single crystals of perchlorates **10a**, **10f**, and **10g** were grown by crystallization from hot AcOH solution. Single-crystal X-ray diffraction experiments were carried out using a SMART APEX2 CCD diffractometer ( $\lambda(\text{Mo-K}\alpha) = 0.71073 \text{ \AA}$ , graphite monochromator,  $\omega$ -scans) at 100 K. Collected data were processed by the SAINT and SADABS programs incorporated into the APEX2 program package [73]. The structures were solved by the direct methods and refined by the full-matrix least-squares procedure against  $F^2$  in anisotropic approximation. The refinement was carried out with the SHELXTL program [74]. The CCDC numbers (2210557 for **10a**, 2210558



for **10f**, and 2210559 for **10g**) contain the supplementary crystallographic data for this paper. These data can be obtained free of charge via [www.ccdc.cam.ac.uk/data\\_request/cif](http://www.ccdc.cam.ac.uk/data_request/cif), accessed on 1 November 2022.

**Crystallographic data for compound 10a:**  $C_7H_7N_6O^+ClO_4^-$  are monoclinic, space group  $P2_1/c$ :  $a = 15.1208(6)$  Å,  $b = 11.7428(5)$  Å,  $c = 20.4811(8)$  Å,  $\beta = 98.7126(13)^\circ$ ,  $V = 3594.7(3)$  Å<sup>3</sup>,  $Z = 12$ ,  $M = 290.64$ ,  $d_{\text{cryst}} = 1.611$  g·cm<sup>−3</sup>.  $wR2 = 0.2394$  calculated on  $F^2_{hkl}$  for all 7199 independent reflections with  $2\theta < 52.5^\circ$  ( $GOF = 1.004$ ,  $R = 0.0680$  calculated on  $F_{hkl}$  for 5235 reflections with  $I > 2\sigma(I)$ ).

**Crystallographic data for compound 10f:**  $C_8H_9N_6O^+ClO_4^-$  are monoclinic, space group  $P2_1/n$ :  $a = 8.1920(3)$  Å,  $b = 13.8353(5)$  Å,  $c = 10.8329(4)$  Å,  $\beta = 91.751(2)^\circ$ ,  $V = 1227.21(8)$  Å<sup>3</sup>,  $Z = 4$ ,  $M = 304.66$ ,  $d_{\text{cryst}} = 1.649$  g·cm<sup>−3</sup>.  $wR2 = 0.0805$  calculated on  $F^2_{hkl}$  for all 2703 independent reflections with  $2\theta < 54.2^\circ$  ( $GOF = 1.050$ ,  $R = 0.0297$  calculated on  $F_{hkl}$  for 2300 reflections with  $I > 2\sigma(I)$ ).

**Crystallographic data for compound 10g:**  $C_8H_{10}N_3O^+ClO_4^-$  are triclinic, space group  $P-1$ :  $a = 11.2823(6)$  Å,  $b = 11.4350(6)$  Å,  $c = 11.6297(6)$  Å,  $\alpha = 98.260(3)^\circ$ ,  $\beta = 118.986(2)^\circ$ ,  $\gamma = 110.895(2)^\circ$ ,  $V = 1130.45(11)$  Å<sup>3</sup>,  $Z = 4$ ,  $M = 263.64$ ,  $d_{\text{cryst}} = 1.549$  g·cm<sup>−3</sup>.  $wR2 = 0.1358$  calculated on  $F^2_{hkl}$  for all 4613 independent reflections with  $2\theta < 52.8^\circ$  ( $GOF = 1.105$ ,  $R = 0.0522$  calculated on  $F_{hkl}$  for 3871 reflections with  $I > 2\sigma(I)$ ).

**3,5,7-Trimethyl-[1,2,5]oxadiazolo [2,3-*a*]pyrimidin-8-ium perchlorate (10a).** A mixture of 58%  $HClO_4$  (0.97 g, 5.6 mmol),  $CF_3CO_2H$  (3.5 mL), and 3-amino-4-methylfuran (0.5 g, 5.0 mmol) was stirred for 5 min at rt, and pentane-2,4-dione (0.56 g, 5.6 mmol) was added. The mixture was stirred for 3 h at rt and then diluted with  $Et_2O$  (20 mL). The precipitate was isolated by filtration, washed with  $EtOH$  ( $3 \times 5$  mL) and  $Et_2O$  ( $2 \times 5$  mL), and dried under vacuum to give salt **10a** (80%) as a white solid: mp 213–214 °C dec [lit. [44] mp 195–197 °C (dec)]; IR (KBr)  $\nu$  3092, 2934, 1629, 1575, 1563, 1442, 1401, 1377, 1363, 1269, 1205, 1094 cm<sup>−1</sup>; <sup>1</sup>H NMR ( $CD_3CN$ )  $\delta$  2.84 (s, 3H), 2.95 (s, 3H), 3.05 (s, 3H), 8.06 (s, 1H); <sup>13</sup>C NMR ( $CD_3CN$ )  $\delta$  9.3, 16.2, 25.6, 122.7, 146.2, 151.1, 154.7, 177.9; <sup>15</sup>N NMR ( $CD_3CN$ )  $\delta$  268.8, 281.0, 389.2; <sup>35</sup>Cl NMR ( $CD_3CN$ )  $\delta$  1012.1. Anal. Calcd for  $C_8H_{10}ClN_3O_5$  (263.63): C, 36.45; H, 3.82; N, 15.94. Found: C, 36.40; H, 3.79; N, 15.91.

**6-Chloro-3,5,7-trimethyl-[1,2,5]oxadiazolo [2,3-*a*]pyrimidin-8-ium perchlorate (10b).** Following the same procedure outlined above, 3-chloropentane-2,4-dione gave the desired product **10b** (85%) as a white solid: mp 180–181 °C dec; IR (KBr)  $\nu$  3026, 2934, 1605, 1552, 1395, 1266, 1095 cm<sup>−1</sup>; <sup>1</sup>H NMR ( $CD_3CN$ )  $\delta$  2.63 (s, 3H), 3.02 (s, 3H), 3.14 (s, 3H); <sup>13</sup>C NMR ( $CD_3CN$ )  $\delta$  8.9, 15.2, 25.1, 132.1, 143.4, 149.3, 154.5, 175.1. Anal. Calcd for  $C_8H_9Cl_2N_3O_5$  (298.08): C, 32.24; H, 3.04; N, 14.10. Found: C, 32.29; H, 3.07; N, 14.05.

**3-Chloromethyl-5,7-dimethyl-[1,2,5]oxadiazolo [2,3-*a*]pyrimidin-8-ium perchlorate (10e).** Following the same procedure outlined above, the reaction of 3-amino-4-chloromethylfuran (**9b**) with pentane-2,4-dione gave the desired product **10e** (96%) as a white solid: mp 195–196 °C dec; IR (KBr)  $\nu$  3076, 3023, 2932, 1626, 1572, 1441, 1396, 1377, 1262, 1202, 1093, 779, 738, 625 cm<sup>−1</sup>; <sup>1</sup>H NMR ( $CD_3CN$ )  $\delta$  2.98 (s, 3H), 3.02 (s, 3H), 3.08 (s, 3H), 5.21 (s, 2H), 8.12 (s, 1H); <sup>13</sup>C NMR ( $CD_3CN$ )  $\delta$  15.3, 24.8, 31.8, 122.4, 143.7, 150.6, 153.0, 177.7. Anal. Calcd for  $C_8H_9Cl_2N_3O_5$  (298.08): C, 32.24; H, 3.04; N, 14.10. Found: C, 32.21; H, 3.02; N, 14.06.

**3-Azidomethyl-5,7-dimethyl-[1,2,5]oxadiazolo [2,3-*a*]pyrimidin-8-ium perchlorate (10f).** Following the same procedure, the reaction of 3-amino-4-azidomethylfuran (**9c**) with pentane-2,4-dione gave the desired product **10f** (94%) as a white solid: mp 195–196 °C dec; IR (KBr)  $\nu$  3081, 2934, 2215, 2125, 1624, 1573, 1442, 1424, 1333, 1282, 1264, 1195, 1093 cm<sup>−1</sup>; <sup>1</sup>H NMR ( $CD_3CN$ )  $\delta$  2.93 (s, 3H), 3.05 (s, 3H), 3.08 (s, 3H), 5.04 (s, 2H), 8.08 (s, 1H); <sup>13</sup>C NMR ( $CD_3CN$ )  $\delta$  14.5, 23.9, 42.2, 121.4, 143.3, 149.7, 151.7, 176.7. Anal. Calcd for  $C_8H_9ClN_6O_5$  (304.65): C, 31.54; H, 2.98; N, 27.59. Found: C, 31.60; H, 3.03; N, 27.56.

**3-Azido-5,7-dimethyl-[1,2,5]oxadiazolo [2,3-*a*]pyrimidin-8-ium perchlorate (10g).** Following the same procedure, the reaction of 3-amino-4-azidofuran (**9d**) with pentane-2,4-dione gave the desired product **10g** (71%) as a white solid: mp 140–141 °C dec; IR (KBr)  $\nu$  3082, 2930, 2157, 1625, 1543, 1443, 1412, 1306, 1266, 1177, 1091 cm<sup>−1</sup>; <sup>1</sup>H NMR ( $CD_3CN$ )



$\delta$  2.96 (s, 3H), 3.05 (s, 3H), 8.13 (s, 1H);  $^{13}\text{C}$  NMR ( $\text{CD}_3\text{CN}$ )  $\delta$  15.9, 25.6, 123.5, 140.8, 152.0, 153.0, 178.2. Anal. Calcd for  $\text{C}_7\text{H}_7\text{ClN}_6\text{O}_5$  (290.62): C, 28.93; H, 2.43; N, 28.92. Found: C, 29.00; H, 2.47; N, 28.86.

#### 4. Conclusions

A new group of furazan-based energetic materials, [1,2,5]oxadiazolo [2,3-*a*]pyrimidin-8-ium perchlorates bearing explosophoric groups, have been synthesized for the first time. The synthetic protocol does not require complex procedures, relying on the simple mixing of available reagents and the usual filtering of the desired product. All compounds were fully characterized by multinuclear NMR spectroscopy and X-ray crystal structure determinations. Initial safety testing (impact and friction sensitivity) and thermal stability measurements (DTA) were also carried out. These salts demonstrate an excellent burn rate and combustion behavior. Considering the simplicity of preparation and the inherent combination of properties, the [1,2,5]oxadiazolo [2,3-*a*]pyrimidin-8-ium backbone may be used as an effective building block in the creation of new energetic materials for various purposes.

**Supplementary Materials:** The following supporting information can be downloaded at: <https://www.mdpi.com/article/10.3390/molecules27238443/s1>. Figures of thermograms for decomposition in non-isothermal conditions, curves of decomposition in isothermal conditions, estimation of standard (solid-state) enthalpies of formation, and copies of NMR spectra are available in supplementary information. Figure S1. Figure S2. TGA and DSC curves of compound **10g** at a heating rate  $10\text{ }^\circ\text{C min}^{-1}$ . Figure S3. TGA and DSC curves of compound **10f** at a heating rate  $10\text{ }^\circ\text{C min}^{-1}$ . Table S1. Results of DSC study for compounds of this study. Figure S4. Gas release curves of compound **10a** at different temperatures. Points are experiment, lines are fittings. Figure S5. Gas release curves of compound **10f** at different temperatures. Points are experiment, lines are fittings. Figure S6. Figure S7. Comparison of decomposition kinetic data for compounds **10a**, **10f**, **10g** and tetrazene obtained in non isothermal (DSC, triangles) and isothermal (Manometry, points) conditions. Figure S8. Effect of Hammett constants of substituent constants at the 1,2,5-oxadiazole ring on the decomposition rate in liquid and solid state. Temperature is  $150\text{ }^\circ\text{C}$ . Figure S9. The Born-Haber thermodynamic cycle employed for the estimation of the formation enthalpy of the crystalline salts **10a**, **10f**, and **10g**. Table S2. The Thermochemical Properties of compounds **10a**, **10f**, and **10g**. Points are experiment, lines are fittings. Refs. [75–89] are cited in the Supplementary Materials.

**Author Contributions:** Conceptualization, V.P.S. and A.B.S.; methodology, K.V.S. and A.B.S.; investigation, K.V.S., A.D.S., S.A.F., A.I.S., K.Y.S., K.A.M. and V.G.K.; writing—original draft, V.P.S., K.V.S. and K.Y.S.; writing—review and editing, V.P.S. and A.B.S.; project administration, A.B.S.; funding acquisition, A.B.S. All authors have read and agreed to the published version of the manuscript.

**Funding:** This research was supported by the Russian Science Foundation (grant no. 20-13-00289).

**Institutional Review Board Statement:** Not applicable.

**Informed Consent Statement:** Not applicable.

**Data Availability Statement:** CCDC 2210557, 2210558 and 2210559 contain the supplementary crystallographic data for this paper. The data can be obtained free of charge from The Cambridge Crystallographic Data Centre via <https://www.ccdc.cam.ac.uk/structures>.

**Acknowledgments:** The authors thank the Department of Structural Studies of the Zelinsky Institute of Organic Chemistry for X-ray analyses of compound **10g**. Single-crystal X-ray study of compounds **10a** and **10f** and crystal structure analysis were supported by the Ministry of Science and Higher Education of the Russian Federation (Contract/Agreement No. 075-00697-22-00).

**Conflicts of Interest:** The authors declare no conflict of interest. The funders had no role in the design of the study; in the collection, analyses, or interpretation of data; in the writing of the manuscript, or in the decision to publish the results.

**Sample Availability:** Since all the compounds in this study are potentially dangerous, the authors do not assume responsibility for providing these samples. On the other hand, a description of the preparation of all compounds can be found in the manuscript and in the Supplementary Materials.

## References

1. Rogov, N.G.; Ischenko, M.A. *Solid Composite Propellants: Components, Requirements, Properties*; SPSTU: St. Petersburg, Russia, 2005. (In Russian)
2. Madyakin, F.P. *Components and Combustion Products of Pyrotechnic Compositions*; KSTU: Kazan, Russia, 2006. (In Russian)
3. Singh, H.; Shekhar, H. *Solid Rocket Propellants: Science and Technology Challenges*; Royal Society of Chemistry: London, UK, 2017.
4. Zhang, L.; Lin, Q.-Q.; Cheng, B.; Wang, P.; Lu, M.; Lin, Q.-H. Effect of hexanitroethane (HNE) and hydrazinium nitroformate (HNF) on energy characteristics of composite solid propellants. *FirePhysChem* **2021**, *1*, 116–122. [\[CrossRef\]](#)
5. Gao, H.; Shreeve, J.M. Azole-Based Energetic Salts. *Chem. Rev.* **2011**, *111*, 7377–7436. [\[CrossRef\]](#) [\[PubMed\]](#)
6. Zhang, Q.; Shreeve, J.M. Energetic Ionic Liquids as Explosives and Propellant Fuels: A New Journey of Ionic Liquid Chemistry. *Chem. Rev.* **2014**, *114*, 10527–10574. [\[CrossRef\]](#)
7. Sebastiao, E.; Cook, C.; Hub, A.; Murugesu, M. Recent developments in the field of energetic ionic liquids. *J. Mater. Chem. A* **2014**, *2*, 8153–8173. [\[CrossRef\]](#)
8. Chingin, K.; Perry, R.H.; Chambreau, S.D.; Vaghjiani, G.L.; Zare, R.N. Generation of melamine polymer condensates upon hypergolic ignition of dicyanamide ionic liquids. *Angew. Chem. Int. Ed.* **2011**, *50*, 8634–8637. [\[CrossRef\]](#) [\[PubMed\]](#)
9. Sheremetev, A.B. Zelinsky Institute of Organic Chemistry, Russian Academy of Sciences, Moscow, Russia. 2001; Unpublished work.
10. Dorofeenko, G.N.; Krivun, S.V.; Dulenkov, V.I.; Zhdanov, Y.A. Perchloric acid and its compounds in organic synthesis. *Russ. Chem. Rev.* **1965**, *34*, 88–104, [Translation of *Usp. Khim.* **1965**, *34*, 219–252]. [\[CrossRef\]](#)
11. Deshpande, S.S.; Kumar, A. Activation of Organic Reactions by Perchlorates. *Adv. Org. Synth.* **2005**, *1*, 215–232. [\[CrossRef\]](#)
12. Dalpozzo, R.; Bartoli, G.; Sambri, L.; Melchiorre, P. Perchloric Acid and Its Salts: Very Powerful Catalysts in Organic Chemistry. *Chem. Rev.* **2010**, *110*, 3501–3551. [\[CrossRef\]](#) [\[PubMed\]](#)
13. Sheremetev, A.B.; Makhova, N.N.; Friedrichsen, W. Monocyclic Furazans and Furoxans. *Adv. Heterocycl. Chem.* **2001**, *78*, 65–188. [\[CrossRef\]](#)
14. Fershtat, L.L.; Makhova, N.N. 1,2,5-Oxadiazole-Based High-Energy-Density Materials: Synthesis and Performance. *ChemPlusChem* **2020**, *85*, 13–42. [\[CrossRef\]](#)
15. Zhang, J.; Zhou, J.; Bi, F.; Wang, B. Energetic materials based on poly furazan and furoxan structures. *Chin. Chem. Lett.* **2020**, *31*, 2375–2394. [\[CrossRef\]](#)
16. Li, Y.; Yuan, J.M.; Zhao, W.; Qu, Y.; Xing, X.W.; Meng, J.W.; Liu, Y.C. Application and Development of 3,4-Bis(3-nitrofurazan-4-yl)furoxan (DNFTF). *Russ. J. Gen. Chem.* **2021**, *91*, 445–455. [\[CrossRef\]](#)
17. Tang, J.; Yang, H.; Cui, Y.; Cheng, G. Nitrogen-rich tricyclic-based energetic materials. *Mater. Chem. Front.* **2021**, *5*, 7108–7118. [\[CrossRef\]](#)
18. Willer, R.L.; Day, R.S.; Park, D.J. Composition of Salts of 3-Nitramino-4-Nitrofurazan for Propellants. U.S. Patent 5,460,669, 28 June 1995.
19. Williams, G.K.; Brill, T.B. Thermal decomposition of energetic materials 72: Unusual behavior of substituted furazan compounds upon flash pyrolysis. *Combust. Flame* **1998**, *114*, 569–576. [\[CrossRef\]](#)
20. Sheremetev, A.B.; Yudin, I.L.; Aleksandrova, N.S.; Aronova, S.M.; Kryazhevskikh, I.A.; Lempert, D.B. Hydroxylammonium salts of furazan family. *Int. Annu. Conf. ICT* **2003**, *34*, 101/1–101/10.
21. Blomquist, H.R. (Nitramino)Nitrofurazan-Based Monopropellant Smokeless Gas Generating Compositions, Especially for Airbags. U.S. Patent 6,513,834, 29 August 2003.
22. Wang, B.; Xiong, H.; Cheng, G.; Yang, H. Incorporating Energetic Moieties into Four Oxadiazole Ring Systems for the Generation of High-Performance Energetic Materials. *ChemPlusChem* **2018**, *83*, 439–447. [\[CrossRef\]](#)
23. Ma, J.; Chinnam, A.K.; Cheng, G.; Yang, H.; Zhang, J.; Shreeve, J.M. 1,3,4-Oxadiazole Bridges: A Strategy to Improve Energetics at the Molecular Level. *Angew. Chem. Int. Ed.* **2021**, *60*, 5497–5504. [\[CrossRef\]](#) [\[PubMed\]](#)
24. Sheremetev, A.B. (Perchlorylamino)furazans and its salts: New high-energy-density materials with high sensitivity. *Mendeleev Commun.* **2020**, *30*, 490–493. [\[CrossRef\]](#)
25. Li, H.; Zhao, F.; Wang, B.; Zhai, L.; Lai, W.; Liu, N. A new family of energetic salts based on oxybridged bis(dinitromethyl)furazan: Syntheses, characterization and properties. *RSC Adv.* **2015**, *5*, 21422–21429. [\[CrossRef\]](#)
26. Zhai, L.; Fan, X.; Wang, B.; Bi, F.; Liab, Y.; Zhua, Y. A green high-initiation-power primary explosive: Synthesis, 3D structure and energetic properties of dipotassium 3,4-bis(3-dinitromethylfurazan-4-oxy)furazan. *RSC Adv.* **2015**, *5*, 57833–57841. [\[CrossRef\]](#)
27. Tang, Y.; Gao, H.; Imler, G.H.; Parrish, D.A.; Shreeve, J.M. Energetic dinitromethyl group functionalized azofurazan and its azofurazanates. *RSC Adv.* **2016**, *6*, 91477–91482. [\[CrossRef\]](#)
28. Huang, H.; Li, Y.; Yang, J.; Pan, R.; Lin, X. Materials with good energetic properties resulting from the smart combination of nitramino and dinitromethyl group with furazan. *New J. Chem.* **2017**, *41*, 7697–7704. [\[CrossRef\]](#)
29. Ma, Q.; Gu, H.; Huang, J.; Liu, D.; Li, J.; Fan, G. Synthesis and Characterization of New Melt-cast Energetic Salts: Dipotassium and Diaminoguanidinium N,N'-Dinitro-N,N'-Bis(3-dinitromethyl-furazanate-4-yl)methylenediamine. *Propellants Explos. Pyrotech.* **2018**, *43*, 90–95. [\[CrossRef\]](#)
30. Guo, T.; Wang, Z.; Tang, W.; Wang, W.; Bi, F.; Wang, B.; Zhou, Z.; Meng, Z.; Ge, Z. A good balance between the energy density and sensitivity from assembly of bis(dinitromethyl) and bis(fluorodinitromethyl) with a single furazan ring. *J. Anal. Appl. Pyrolysis* **2018**, *134*, 218–230. [\[CrossRef\]](#)

31. Yu, Q.; Chinnam, A.K.; Yin, P.; Imler, G.H.; Parrish, D.A.; Shreeve, J.M. Finding furoxan rings. *J. Mater. Chem. A* **2020**, *8*, 5859–5864. [\[CrossRef\]](#)
32. Zhou, Y.; Gao, H.; Shreeve, J.M. Dinitromethyl groups enliven energetic salts. *Energ. Mater. Front.* **2020**, *1*, 2–15. [\[CrossRef\]](#)
33. Wang, B.; Zhang, G.; Huo, H.; Fan, Y.; Fan, X. Synthesis, characterization and thermal properties of energetic compounds derived from 3-amino-4-(tetrazol-5-yl)furazan. *Chin. J. Chem.* **2011**, *29*, 919–924. [\[CrossRef\]](#)
34. Ilyushin, M.A.; Shugaley, I.V.; Tselinskii, I.V.; Garabadzhiu, A.V. Environmental Problems and Their Solutions of Using Energy-Rich Substances for Initiating Devices. *Russ. J. Gen. Chem.* **2013**, *83*, 2624–2632. [\[CrossRef\]](#)
35. Ilyushin, M.A.; Tselinsky, I.V.; Shugalei, I.V. Environmentally Friendly Energetic Materials for Initiation Devices. *Cent. Eur. J. Energ. Mater.* **2012**, *9*, 293–327.
36. Stepanov, A.I.; Sannikov, V.S.; Dashko, D.V.; Roslyakov, A.G.; Astrat'yev, A.A.; Stepanova, E.V.; Aliev, Z.G.; Goncharov, T.K.; Aldoshin, S.M. Synthesis and properties of 3-azido-4-(2H-tetrazol-5-yl)furazan. *Chem. Heterocycl. Compd.* **2017**, *53*, 779–785. [\[CrossRef\]](#)
37. Dong, Z.; An, D.; Yang, R.; Ye, Z. Insensitive and Thermostable Energetic Materials Based on 3-Ureido-4-tetrazole-furazan: Synthesis, Characterization, and Properties. *Z. Anorg. Allg. Chem.* **2019**, *645*, 1285–1290. [\[CrossRef\]](#)
38. Yu, Q.; Yang, H.; Ju, X.; Lu, C.; Lin, Q.; Zhang, J.; Cheng, G. 1D Energetic Metal-Organic Framework: Sodium 6-Nitro-5-oxidopyrazolo [3,4-c][1,2,5]oxadiazol-4-ide with Good Thermal Stability. *ChemistrySelect* **2017**, *2*, 4673–4677. [\[CrossRef\]](#)
39. Tang, Y.; He, C.; Shreeve, J.M. A furazan-fused pyrazole N-oxide via unusual cyclization. *J. Mater. Chem. A* **2017**, *5*, 4314–4319. [\[CrossRef\]](#)
40. Hermann, T.S.; Klapotke, T.M.; Krumm, B. Formation and Characterization of Heavy Alkali and Silver Salts of the 4-Nitro-pyrazolo-(3,4-c)-furazan-5-N-oxide Anion. *Propellants Explos. Pyrotech.* **2018**, *43*, 54–61. [\[CrossRef\]](#)
41. Voronin, A.A.; Fedyanin, I.V.; Churakov, A.M.; Pivkina, A.N.; Muravyev, N.V.; Strelenko, Y.A.; Klenov, M.S.; Lempert, D.B.; Tartakovsky, V.A. 4H-[1,2,3]Triazolo [4,5-c][1,2,5]oxadiazole 5-oxide and Its Salts: Promising Multipurpose Energetic Materials. *ACS Appl. Energy Mater.* **2020**, *3*, 9401–9407. [\[CrossRef\]](#)
42. Sheremetev, A.B.; Yudin, I.L.; Aleksandrova, N.S. High nitrogen furazan derivatives for gas generators. In Proceedings of the Twenty-Third International Pyrotechnics Seminar, Tsukuba, Japan, 30 September 1997; pp. 377–388.
43. Davis, M.; Deady, L.W.; Homfeld, E. Rates of N-methylation of 2-Methylbenzotriazole, 2,1,3-Benzoxadiazole, 2,1,3-Benzothia(or Seleno)diazole, 1,2,5-Oxadiazole and 1,2,5-Thiadiazole. *Aust. J. Chem.* **1974**, *27*, 1917–1921. [\[CrossRef\]](#)
44. Bachkovsky, I.P.; Mikhailovsky, A.P.; Chuiguk, V.A. 1,2,5-Oxadiazolo [2,3-a]-pyrimidinium salts. *Ukr. Khim. Zh.* **1980**, *46*, 637–639.
45. Struchkov, Y.T.; Batsanov, A.S.; Chuiguk, V.A.; Batog, L.V.; Kulikov, A.S.; Pivina, T.S.; Strelenko, Y.A. 5,7-Dimethyl-3-phenylfurazano- and -furoxano [5,4-a]pyrimidinium perchlorates: A new type of condensed system. *Chem. Heterocycl. Comp.* **1992**, *24*, 193–197, [Translation of *Khim. Geterotsikl. Soedin.* **1992**, *2*, 233–238]. [\[CrossRef\]](#)
46. Zhou, J.; Zhang, J.; Wang, B.; Qiu, L.; Sheremetev, A.B. Recent Synthetic Efforts towards High Energy Density Materials: How to Design High-Performance Energetic Structures? *FirePhysChem* **2022**, *2*, 83–139. [\[CrossRef\]](#)
47. Sheremetev, A.B.; Shamshina, Y.L.; Dmitriev, D.E. Synthesis of 3-alkyl-4-aminofurazans. *Russ. Chem. Bull.* **2005**, *54*, 1032–1037, [Translation of *Izv. Akad. Nauk. Ser. Khim.* **2005**, *4*, 1007–1012]. [\[CrossRef\]](#)
48. Sheremetev, A.B.; Mel'nikova, S.F.; Kokareva, E.S.; Nekrutenko, R.E.; Strizhenko, K.V.; Suponitsky, K.Y.; Pham, T.D.; Pivkina, A.N.; Sinditskii, V.P. Nitroxy- and azidomethyl azofurazans as advanced energetic materials. *Def. Technol.* **2022**, *18*, 1369–1381. [\[CrossRef\]](#)
49. Tselinskii, I.V.; Mel'nikova, S.F.; Vergizov, S.N. Azidofurazans in the synthesis of condensed systems. *Zhurnal Org. Khimii* **1981**, *17*, 1123–1124.
50. Rakitin, O.A.; Zalesova, O.A.; Kulikov, A.S.; Makhova, N.N.; Godovikova, T.I.; Khmel'nikskii, L.I. Synthesis and reactivity of furazanyl- and furoxanyldiazonium salts. *Russ. Chem. Bull.* **1993**, *42*, 1865–1870, [Translation of *Izv. Akad. Nauk. Ser. Khim.* **1993**, *11*, 1949–1955]. [\[CrossRef\]](#)
51. Novikova, T.S.; Melnikova, T.M.; Kharitonova, O.V.; Kulagina, V.O.; Aleksandrova, N.S.; Sheremetev, A.B.; Pivina, T.S.; Khmel'nikskii, L.I.; Novikov, S.S. An Effective Method for the Oxidation of Aminofurazans to Nitrofurazans. *Mendeleev Commun.* **1994**, *4*, 138–140. [\[CrossRef\]](#)
52. Apasov, E.T.; Sheremetev, A.B.; Dzhetigenov, B.A.; Kalinin, A.V.; Tartakovsky, V.A. Reaction of Silylated Aminonitrofurazan with N-Magnesium Amine Derivatives. *Bull. Russ. Acad. Sci. Div. Chem. Sci.* **1992**, *41*, 1500–1501. [\[CrossRef\]](#)
53. Skibsted, J.; Jakobsen, H.J. <sup>35</sup>Cl and <sup>37</sup>Cl Magic-Angle Spinning NMR Spectroscopy in the Characterization of Inorganic Perchlorates. *Inorg. Chem.* **1999**, *38*, 1806–1813. [\[CrossRef\]](#) [\[PubMed\]](#)
54. Suponitsky, K.Y.; Lyssenko, K.A.; Antipin, M.Y.; Aleksandrova, N.S.; Sheremetev, A.B.; Novikova, T.S. 4,4-Bis(nitramin)azofurazane and its Salts. Study of Molecular and Crystal Structure Based on X-ray and Quantum Chemical Data. *Russ. Chem. Bull.* **2009**, *58*, 2129–2136. [\[CrossRef\]](#)
55. Suponitsky, K.Y.; Lyssenko, K.A.; Ananyev, I.V.; Kozeev, A.M.; Sheremetev, A.B. Role of Weak Intermolecular Interactions in the Crystal Structure of Tetrakis-furazano [3,4-c:3',4'-g:3'',4''-k:3''',4'''-o][1,2,5,6,9,10,13,14]octaazacyclohexadecine and Its Solvates. *Cryst. Growth Des.* **2014**, *14*, 4439–4449. [\[CrossRef\]](#)
56. Suponitsky, K.Y.; Smol'yakov, A.F.; Ananyev, I.V.; Khakhalev, A.V.; Gidasov, A.A.; Sheremetev, A.B. 3,4-Dinitrofurazan: Structural Nonequivalence of Ortho-Nitro Groups as a Key Feature of the Crystal Structure and Density. *ChemistrySelect* **2020**, *5*, 14543–14548. [\[CrossRef\]](#)

57. Manelis, G.B.; Nazin, G.M.; Rubtsov, Y.I.; Strunin, V.A. *Thermal Decomposition and Combustion of Explosives and Propellants*; CRC Press: London, UK, 2003. [CrossRef]
58. Sinditskii, V.P.; Burzhava, A.V.; Sheremetev, A.B.; Aleksandrova, N.S. Thermal and combustion properties of 3,4-Bis(3-nitrofurazan-4-yl)furoxan (DNTF). *Propellants Explos. Pyrotech.* **2012**, *37*, 575–580. [CrossRef]
59. Sinditskii, V.P.; Burzhava, A.V.; Egorshv, V.Y.; Sheremetev, A.B.; Zelenov, V.P. Combustion of Furazanotetrazine Dioxide. *Combust. Explos. Shock. Waves* **2013**, *49*, 117–120, [Translation of *Fiz. Goren. Vzriv.* **2013**, *49*, 134–137]. [CrossRef]
60. Sinditskii, V.P.; Burzhava, A.V.; Chernyi, A.N.; Shmelev, D.S.; Apalkova, V.N.; Palysaeva, N.V.; Sheremetev, A.B. A comparative study of two difurazanyl ethers. *J. Therm. Anal. Calorim.* **2016**, *123*, 1431–1438. [CrossRef]
61. Sinditskii, V.P.; Smirnova, A.D.; Serushkin, V.V.; Aleksandrova, N.S.; Sheremetev, A.B. Furazan-fused azacyclic nitramines: Influence of structural features on the combustion and the thermolysis. *ChemistrySelect* **2020**, *5*, 13868–13877. [CrossRef]
62. Sinditskii, V.P.; Burzhava, A.V.; Sheremetev, A.B. Macrocyclic tetra(azo-) and tetra(azoxyfurazan)s: Comparative study of decomposition and combustion with linear analogs. *Energetic Mater. Front.* **2021**, *2*, 87–95. [CrossRef]
63. Sinditskii, V.P.; Smirnova, A.D.; Serushkin, V.V.; Yudin, N.V.; Vatsadze, I.A.; Dalinger, I.L.; Kiselev, V.G.; Sheremetev, A.B. Nitroderivatives of N-pyrazolyltetrazoles: Thermal decomposition and combustion. *Thermochim. Acta* **2021**, *698*, 178876. [CrossRef]
64. Vereschagin, A.N. *Inductive Effect. Constants of Substituents for Correlation Analysis*; Nauka: Moscow, Russia, 1988.
65. Whelan, D.J.; Spear, R.J.; Read, R.W. The thermal decomposition of some primary explosives as studied by differential scanning calorimetry. *Thermochim. Acta* **1984**, *80*, 149–163. [CrossRef]
66. Sinditskii, V.P.; Egorshv, V.Y.; Berezin, M.V.; Serushkin, V.V. Mechanism of HMX combustion in a wide range of pressures. *Combust. Explos. Shock. Waves* **2009**, *45*, 461–477. [CrossRef]
67. Fogelzang, A.E.; Egorshv, V.Y.; Pimenov, A.Y.; Sinditskii, V.P.; Saklanty, A.R.; Svetlov, B.S. Investigation of the Steady-State Burning of Primary Explosives at High Pressures. *Dokl. Akad. Nauk SSSR* **1985**, *285*, 1449–1452.
68. Sinditskii, V.P.; Egorshv, V.Y.; Serushkin, V.V.; Levshenkov, A.I.; Berezin, M.V.; Filatov, S.A. Combustion of energetic materials governed by reactions in the condensed phase. *Inter. J. Ener. Mat. Chem. Prop.* **2010**, *9*, 147–192. [CrossRef]
69. Kolesov, V.I.; Kapranov, K.O.; Tkacheva, A.V.; Kulagin, I.A. Explosive Characteristics of Tetrazene and MTX-1. *Combust. Explos. Shock Waves* **2021**, *57*, 350–355. [CrossRef]
70. Muravyev, N.V.; Wozniak, D.R.; Piercey, D.G. Progress and performance of energetic materials: Open dataset, tool, and implications for synthesis. *J. Mater. Chem. A* **2022**, *10*, 11054–11073. [CrossRef]
71. STANAG 4489; Explosives, Impact Sensitivity Tests. NATO: Brussels, Belgium, 1999.
72. STANAG 4487; Explosives, Friction Sensitivity Tests. NATO: Brussels, Belgium, 2002.
73. Bruker AXS Inc. *APEX2 and SAINT*; Bruker AXS Inc.: Madison, WI, USA, 2014.
74. Sheldrick, G.M. Crystal structure refinement with SHELXL. *Acta Cryst. C* **2015**, *71*, 3–8. [CrossRef] [PubMed]
75. Kissinger, H.E. Reaction kinetics in differential thermal analysis. *Anal. Chem.* **1957**, *29*, 1702–1706. [CrossRef]
76. Jenkins, H.D.B.; Roobottom, H.K.; Passmore, J.; Glasser, L. Relationships among Ionic Lattice Energies, Molecular (Formula Unit) Volumes, and Thermochemical Radii. *Inorg. Chem.* **1999**, *38*, 3609–3620. [CrossRef]
77. Jenkins, H.D.B.; Tudela, D.; Glasser, L. Lattice Potential Energy Estimation for Complex Ionic Salts from Density Measurements. *Inorg. Chem.* **2002**, *41*, 2364–2367. [CrossRef]
78. Curtiss, L.A.; Raghavachari, K.; Redfern, P.C.; Pople, J.A. Assessment of Gaussian-2 and density functional theories for the computation of enthalpies of formation. *J. Chem. Phys.* **1997**, *106*, 1063. [CrossRef]
79. Frisch, M.J.; Trucks, G.W.; Schlegel, H.B.; Scuseria, G.E.; Robb, M.A.; Cheeseman, J.R.; Scalmani, G.; Barone, V.; Petersson, G.A.; Nakatsuji, H.; et al. *Gaussian 09, Revision D.01*; Gaussian, Inc.: Wallingford, CT, USA, 2016.
80. Werner, H.-J.; Knowles, P.J.; Knizia, G.; Manby, F.R.; Schutz, M.; Celani, P.; Korona, T.; Lindh, R.; Mitrushenkov, A.; Rauhut, G.; et al. MOLPRO, Version 2010.1. *Users Man. Version*. 2010. Available online: <https://www.molpro.net/pipermail/molpro-user/2010-September/003868.html> (accessed on 1 November 2022).
81. Karton, A.; Martin, J.M.L. Explicitly correlated Wn theory: W1-F12 and W2-F12. *J. Chem. Phys.* **2012**, *136*, 124114. [CrossRef]
82. Kesharwani, M.K.; Brauer, B.; Martin, J.M.L. Frequency and Zero-Point Vibrational Energy Scale Factors for Double-Hybrid Density Functionals (and Other Selected Methods): Can Anharmonic Force Fields Be Avoided? *J. Phys. Chem. A* **2015**, *119*, 1701–1714. [CrossRef]
83. Karton, A.; Schreiner, P.R.; Martin, J.M.L. Heats of formation of platonic hydrocarbon cages by means of high-level thermochemical procedures. *J. Comput. Chem.* **2016**, *37*, 49–58. [CrossRef]
84. Kiselev, V.G.; Goldsmith, C.F. Accurate Prediction of Bond Dissociation Energies and Barrier Heights for High-Energy Caged Nitro and Nitroamino Compounds Using a Coupled Cluster Theory. *J. Phys. Chem. A* **2019**, *123*, 4883–4890. [CrossRef] [PubMed]
85. Kiselev, V.G.; Goldsmith, C.F. Accurate Thermochemistry of Novel Energetic Fused Tricyclic 1,2,3,4-Tetrazine Nitro Derivatives from Local Coupled Cluster Methods. *J. Phys. Chem. A* **2019**, *123*, 9818–9827. [CrossRef] [PubMed]
86. Gorn, M.V.; Gritsan, N.P.; Goldsmith, C.F.; Kiselev, V.G. Thermal Stability of Bis-Tetrazole and Bis-Triazole Derivatives with Long Catenated Nitrogen Chains: Quantitative Insights from High-Level Quantum Chemical Calculations. *J. Phys. Chem. A* **2020**, *124*, 7665–7677. [CrossRef] [PubMed]



- 
87. Muravyev, N.V.; Monogarov, K.A.; Melnikov, I.N.; Pivkina, A.N.; Kiselev, V.G. Learning to Fly: Thermochemistry of Energetic Materials by Modified Thermogravimetric Analysis and Highly Accurate Quantum Chemical Calculations. *Phys. Chem. Chem. Phys.* **2021**, *23*, 15522–15542. [[CrossRef](#)] [[PubMed](#)]
  88. Lee, T.J.; Taylor, P.R. A diagnostic for determining the quality of single-reference electron correlation methods. *Int. J. Quantum Chem.* **1989**, *36*, 199–207. [[CrossRef](#)]
  89. Chase, M.W., Jr. *NIST-JANAF Thermochemical Tables*; American Chemical Society: Washington, DC, USA, 1998; Volume 9.